Exploring multiple bioprocess monitoring modalities for Large-scale 3D Bioprinted Tissue Cultivation

Laura Chastagnier, Sarah Pragnere, Yilbert Gimènez, Céline Loubière, Naima El-Kholti, Kleanthis Mazarakis, Timo Schmidberger, Eric Olmos, Simon Auguste Lambert, Christophe Marquette, et al.

Exploring multiple bioprocess monitoring modalities for Large-scale 3D Bioprinted Tissue Cultivation

Laura CHASTAGNIER
3d.FAB, CNRS, INSA, CPE-Lyon, UMR5246, ICBMS, Université Claude Bernard Lyon 1
Sarah Pragnere
3d.FAB, CNRS, INSA, CPE-Lyon, UMR5246, ICBMS, Université Claude Bernard Lyon 1
Yilbert Gimènez
3d.FAB, CNRS, INSA, CPE-Lyon, UMR5246, ICBMS, Université Claude Bernard Lyon 1
Céline Loubière
Université de Lorraine, CNRS, LRGP, F-54001 Nancy, France
Naima el-Kholti
UMR 5305, Tissue Biology and Therapeutic Engineering Laboratory (LBTI), University of Lyon, CNRS.
Kleanthis Mazarakis
Sartorius Stedim UK Ltd.
Timo Schmidberger
Sartorius Stedim Biotech GmbH
Eric Olmos
Université de Lorraine, CNRS, LRGP, F-54001 Nancy, France
Simon Auguste Lambert
Univ Lyon, Université Claude Bernard Lyon 1, INSA Lyon, Ecole Centrale de Lyon, CNRS, Ampère, UMR5005
Christophe Marquette
3d.FAB, CNRS, INSA, CPE-Lyon, UMR5246, ICBMS, Université Claude Bernard Lyon 1
Emma Petiot
emma.petiot@univ-lyon1.fr

3d.FAB, CNRS, INSA, CPE-Lyon, UMR5246, ICBMS, Université Claude Bernard Lyon 1

Article

Keywords: Bioreactor, Tissue cultivation, Bioprinting, Online monitoring, Computational Fluid Dynamics (CFD) simulation, Magnetic Resonance Imaging (MRI)

Posted Date: March 25th, 2024

DOI: https://doi.org/10.21203/rs.3.rs-4021195/v1

Additional Declarations: Competing interest reported. Two of the authors Kleanthis Mazarakis & Timo Schmidberger are researcher of a private company (Sartorius) which is selling the SIMCA spectra analysis software used in this study. Also, 3d.FAB team should specify that Sartorius has financially supported part of this work with the hiring of Laura Chastagnier as a PhD student and contributed to the completion of this work by providing the SIMCA software.

Abstract

In tissue engineering (TE) and regenerative medicine (RM), challenges persist in achieving optimal tissue maturation due to uncontrolled physicochemical environments and the necessity for a dynamic nutrient supply. Real-time monitoring tools are crucial to address these challenges effectively. Our study evaluates nondestructive qualification tools for pre-implantation tissue assessment, aiming to enhance their quality assessment capabilities and broaden their biomedical applications. These tools target internal tissue structure, nutritive medium flow paths, and tissue metabolic state. We extend the capabilities of tissue culture monitoring by integrating advanced bioprocess technologies like Raman spectroscopy or in-vivo imaging tools like magnetic resonance imaging (MRI). Through comparative analysis with Computational Fluid Dynamics (CFD) simulations and MRI velocity mapping, we highlight the synergistic relationship between simulation-based and experimental approaches in optimising tissue feeding and oxygenation. MRI emerges as a precious tool for longitudinal tissue development monitoring, surpassing traditional destructive methods. Our findings underscore the importance of dynamic regulation in tissue culture protocols, facilitated by continuous monitoring and adjustment of the physicochemical tissue environment. Based on evidence from industrial cell-culture processes, Raman spectroscopy emerges as a standard tool for monitoring metabolic tissue. These advancements significantly propel RM and TE, paving the way for comprehensive studies and quantitative analyses essential for developing functional engineered tissues across diverse biomedical applications.

Introduction

While Tissue Engineering (TE) and Regenerative Medicine (RM) have experienced substantial growth over the past decade and have incorporated technologies from various domains to overcome the scientific community’s boundaries, these fields are still struggling with some persisting challenges.

Notably, 3D bioprinting, derived from material additive manufacturing, has made significant progress, achieving unprecedented tissue and organ engineering complexity [1,2]. However, the maturation strategies, encompassing duration, culture media, and incorporating mechanical/hydrodynamic stimulation, remain in their infancy concerning the potential clinical applications of these approaches and present urgent issues that need attention [2].

Maturation protocols are developed with small-scale tissues, often below cm scale, within non-fully controlled physicochemical environments. While studies are conducted in incubators with regulated temperatures, the pH is buffered, and oxygen supply to the tissues is not controlled. To address this, dynamic cultures using perfused bioreactors are essential to respond to cues influencing tissue development and enhancing tissue maturation. Consequently, numerous studies have focused on optimising nutritive flow within cultured tissues [3,4]. Adequate oxygen and nutritional element distributions are crucial for cultivating tissues larger than centimeters to prevent internal cell necrosis. The development of in-house-developed bioreactors of various shapes is the most common solution. Few studies have explored the integration of sensors into cultivation vessels to monitor the tissue's

physicochemical environment [4,5]. Unfortunately, these studies are often case-specific, employing in-house developed equipment and vessels, and lack comprehensive knowledge of regulation protocols.

Contrastingly, cell-culture bioprocessing in pharmaceutical environments benefits from the presence of bioreactors that regulate the cellular environment. Over the past 50 years, commercial equipment, and protocols with control-loop parameters (PID control) have been successfully implemented [6]. Advanced cell culture processes now involve meticulous monitoring of the cell physicochemical environment. Additionally, spectroscopic technologies, developed over the past two decades, offer insights into and control over the biochemical composition of culture media, including cell nutrients and by-product metabolites [7,8]. Consequently, these technologies and expertise are ready to be transferred to the TE and RM fields.

Developing appropriate tools to monitor tissue maturation steps and ultimately qualify tissue quality is foreseen as an impactful step for TE and RM deployment. Indeed, standard qualification of tissue quality targets their cellularity, the tissue's organisation, and functions.

However, existing reference characterisation methods are offline and involve destructive assays, such as histology or immunohistochemistry[9]. These methods necessitate paraffin embedding and tissue slicing. Cellularity and viability are often observed through microscopy imaging with or without labelling. In parallel, various imaging modalities, including standard fluorescence or confocal microscopy, light-sheet-based fluorescence microscopy [10], tomography (PET—positron emission tomography, OPT—optical projection tomography) [11], and their combination with spectroscopic tools like Raman [10], have been evaluated for *in vitro* produced tissue but are limited in scale and depth of analysis. Tissue transparisation allows for greater depth of up to 300 µm, but it is a destructive practice [9,13]. In these cases, the analysed tissue volumes typically range from 10 µm³ to 7 cm³, significantly lower than the targeted tissue sizes in RM [11,12].

The targeted tissue volumes in RM are substantial, often exceeding cubic centimetres, such as kidneys (560 cm³)[13] or livers (900 cm³) [14], and with thickness above 500 µm like in the case of full-thickness skin[15]. Therefore, the scientific community's primary challenge is assessing large and dense objects, and its ultimate goal is to provide analytical tools implemented close to or on the tissue cultivation vessels for real-time monitoring of tissue fate. Various approaches have been tested or considered, but none have been entirely satisfactory. Qualification and characterisation tools must align with *in vivo* measurement techniques. Magnetic Resonance Imaging (MRI) stands out as a reference tool for both *in vivo* and *in vitro* tissue imaging[13,16,17]. Indeed, MRI offers high spatial resolution from 2 mm^3 in the clinical routine down to 300 µm3 in dedicated MRI systems and a high imaging depth of 0.1 mm up to 40 cm [9,13]. MRI has been employed for fluid velocity mapping in an *in vivo* tumour environment. To reach a resolution of 133 mm^3 its capabilities was enhanced using contrast agents [17]. Overall, there is a tradeoff between spatial resolution and penetration depth of the imaging modality. MRI can image living tissues

at a multiscale level down to an ensemble of cells (30 cells, i.e., the scale of a small spheroid) up to the organ scale [18].

Recently, in-house protocols were developed to implement and transfer bioprocess principles to the tissue culture and monitoring. Off-line assays have characterised tissue maturation timelines, including cell growth and metabolic activity profiles [19,20]. The current work explores non-destructive monitoring and qualification tools for controlling the tissue's physicochemical environment, composition, and evolution. The focus is on targeting internal tissue structure, nutrient and oxygen flow paths within 3D architectures, and the metabolic state of the tissue in a non-destructive, non-contact manner to propose qualification tools for late-stage tissue assessment pre-implantation.

Methods

3D bioprinting of tissue

Cell culture

Three cell types were chosen for this study: human dermal fibroblasts (obtained from Hospice Civil Lyon cell bank, France), HEK293T cells (provided by Dr. C. Maisse-Paradisi, INRA-UCBL-EPHE "Viral Infections and Comparative Pathology", Lyon, France), and CHO DG44 cells (Cellca-Sartorius; PTN1-CB-CC1). The CHO DG44 cell line is deficient in dihydrofolate reductase (DHFR) and has been co-transfected with an exogenous DHFR gene along with a transgene encoding a recombinant protein of interest. This cell line is widely utilised for recombinant protein production due to its ease of selecting high-producing clones with methotrexate (MTX).

Fibroblasts and HEK293T were cultured in Dulbecco's Modified Eagle Medium (DMEM) (Thermo Fisher Scientific, 31966-021) supplemented with 10% (v/v) FBS (Gibco Cell Culture, 10270-106). In bioreactor cultures, the medium was supplemented with 0.5% (v/v) Penicillin-Streptomycin at 10,000 U/mL (Thermo Fisher Scientific, 15140122) and 0.4% (v/v) Amphotericin B (Thermo Fisher Scientific, 15290-018). Cells were precultured at 5% CO_2, 80% humidity and 37°C before bioprinting. Fibroblasts and HEK293T were passaged once and twice a week.

CHO cells were amplified in suspension with 4Cell® Xtra CHO Stock and Amplification Medium (SAM) (Sartorius, CQP3FA1114) serum-free medium prepared supplemented with 6 mM GlutaMAX™ (Gibco, 35050061). Working cell banks were thawed in 10 mL fresh Stock & Adaptation Medium supplemented with 15 nM methotrexate (MTX) (Sigma-Aldrich, M8407) at 4°C and centrifuged at 190 g for 3 min. Cells were then expanded in shake flasks from 50 to 150 mL in SAM medium at 37°C and 7.5% CO_2 and agitated at 130 rpm. They were seeded at a concentration of 0.2 x 10^6 cells/mL and passaged twice a week up to the fifth passage. The medium was supplemented with 15 nM methotrexate for high-producing clone selection only for the first three passages. Viable cell density (VCD) was evaluated by

cell counting on a Malassez Hemocytometer with an exclusion method using Trypan blue (Gibco, 15250061).

3D Macroporous architecture design and 3D printing

3D structures were designed by Computer Assisted Design (CAD) using 3D Builder (Microsoft Corporation). They were sketched to obtain two parallelepipedal macroporous 3D structures of a 10.8 cm^3 total volume (2 x 2 x 2.7 cm). Two distinct internal porosities were produced to challenge our monitoring strategies; one is a 12 x 12 pores geometry with an internal pore size of 1.2 x 1.2 mm(**Supplementary Fig. 1_ design A**), and the second is a 6 x 6 pores geometry of 2.8 x 2.8 mm (**Supplementary Fig. 1_design B**). 3D files were converted to STL format to be transferred to a 3D printer and bioprinter.

Bioprinting of 3D constructs

Bioink formulation was prepared from Fibrinogen, Gelatin and Alginate stock solutions. Stock solutions were prepared by dissolving Fibrinogen 8% w/v (F8630-1G, Merck), Alginate 4% w/v (Alginic acid sodium salt very low viscosity, A18565.36, Alfa Aesar), and Gelatin 20% w/v from porcine skin (G1890 - Sigma Aldrich) in calcium-free DMEM (21068028 - Thermofisher) supplemented with 10% FBS (Gibco). For bioink preparation, trypsinated cells were first resuspended in calcium-free DMEM supplemented with 10% FBS and enumerated. Targeted cell concentration was adjusted by pelleting the appropriate volume of cells at 300 g (Fibroblasts, HEK293T) or 190 g (CHO) for 5 min. The pellet was resuspended in the proper volume of Fibrinogen 8% solution. Bioink was seeded with specific cell concentrations for each cell type (fibroblasts: 1.25 x 10^5 and 2.2 x 10^5 cells/mL; HEK 293T: 2.6 x 10^6 cells/mL of bioink; CHO: 10 x 10^6 cells/mL of bioink).

The appropriate volumes of Alginate 4% solution and Gelatin 20% solutions were added with a final proportion of 25% v/v Fibrinogen stock solution, 50% v/v Alginate stock solution and 25% v/v Gelatin stock solution. It corresponds to a final concentration in the bioink of 2% w/v Fibrinogen, 2% w/v Alginate, and 5% w/v Gelatin. The cells and the three components of the bioink were mixed and homogenised with a viscous-liquid pipet. The bioink was then incubated for 10 min at 37°C before being poured into a printing sterile barrel. The bioink was then incubated for 30 minutes at room temperature (21°C) before being used for 3D bioprinting.

The cellularized macroporous structures (design A or B_**Supplementary Data 1**) were bioprinted at 21°C by pneumatic micro-extrusion (20–50 psi) using a BioAssemblyBot 3D bioprinter (Advanced Solutions, Inc). Printing needles of 800 µm diameter were used. The printing speed was set at 8 mm/s, and the acceleration of the printing nozzle was set at 300 mm/s^2. The bioprinted constructs were consolidated with various solutions depending on the cell types. This solution was composed of transglutaminase (TAG) (ACTIVA WM - Ajinomoto), thrombin from bovine plasma (t4648-10KU - Merck) and $CaCl_2$ (C5670-500G - Merck). The respective concentrations are presented in Table 1. The consolidation process was

carried out at 37°C for 2 hours. The cellularised structures were then rinsed twice with sterile physiological serum (Versol, France) at a 10 mL physiological serum ratio for 1 mL of tissue.

Table 1
_ Respective Consolidation conditions for separated cell lines.

Cell line	Transglutaminase w/v	Calcium Chloride w/v	Thrombin U/ml
Dermis fibroblast	4	3	10
HEK293T	4	3	10
CHO DG44	0.4	1.4	10

Tissue Culture in a Regulated Environment

Bioprocess cultivation set-up

A controlled and regulated physicochemical tissue environment was established using a commercial regulation vessel and a 3D-printed perfused tissue culture chamber (Fig. 1.**a**). This setup, tailored to the tissue's requirements, incorporated a regulation vessel visible on Fig. 1.**b** (Eppendorf DASbox® 250mL glass tank) or Sartorius single-use Ambr®250 Mammalian filterless vessels (001-5G25)) equipped with a heating system and probes for pH, oxygen, and temperature. A circulation loop delivered media from the regulation vessel to the 3D-printed tissue culture chamber (Fig. 1.**a & c**).

To apply control of the culture parameters (pH, dissolved oxygen, temperature), two controllers were employed: a custom Cytosys controller (Ipratech, Belgium) (Fig. 1-a : setup A) and the fully equipped Ambr®250 High Throughput bioreactor system (Sartorius) (Fig. 1-a : setup B). Both system controllers featured peristaltic pumps, a gas injecting port (air, CO_2, N_2), and ports connecting oxygen, pH, and temperature probes. The particularity of the Cystosys controller was to necessitate the integration of an Applikon heating jacket 30W MINIBIO 250 heating blanket, Applikon), a custom stirrer motor, 12 mm pH & dissolved oxygen probes (Hamilton) and two temperature probes (Pt100). The dissolved oxygen regulation loop involved air and nitrogen injections, while pH was regulated thanks to gaseous CO_2 or NaOH 0.2 M solution.

Before cultivation, systems were sterilised by autoclaving or by following the Cleaning in place (CIP) and Sanitization in place (SIP) procedures recommended for the Ambr®250 High Throughput system (Sartorius). Once installed and connected to the controllers, culture regulation vessels were filled with medium a day before the culture, and regulation started to stabilise the probe response before the culture. Once bioprinted and consolidated, the 3D cellularised constructs were sterilely inserted into the perfused 3D printed culture chamber under laminar flow. The culture chamber was sealed with a silicone seal and connected to perfusion tubing. A peristaltic pump from the controller generated perfusion flow

by pumping regulated media from regulation vessels at a 2 or 20 mL/min perfusion rate. A control loop regulates the pH, dissolved oxygen concentration, and temperature.

Additionally, to this culture set-up, in the case of the development of monitoring of metabolite, an extra Raman spectroscopy probe (bIO-LAB 220; Endress + Hauser) coupled to the Rxn2 Raman analyser (Endress + Hauser) was installed in the DASbox® tank (Fig. 1.a).

Design & fabrication of the tissue culture chamber

Computer Assisted Design (CAD) design of the printed perfused vessel was performed using the 3D modelling software Autodesk® Fusion 360™. 3D CAD files were converted to .STL format to be transferred to 3D printer equipment. The vessel was printed in VeroClear (Stratasys) material using an Object30 Pro inkjet printer (Stratasys). Support and unpolymerised material were removed using a Waterjet (Stratasys). The printed vessel was then incubated overnight in 70% ethanol at room temperature to remove all released compounds. After incubation in ethanol, the vessel was rinsed in deionised water.

Tissue Metabolic Activity Monitoring

Enzymatic lactic acid quantification

Spent media were recovered daily through sampling, aliquoted in triplicate and stored at -20°C. These samples were further used to quantify the lactic acid produced by cell metabolism using the L-Lactic Acid Assay from Megazyme (L-Lactic Acid Assay Kit, K-LATE, Megazyme). The assay was performed in 96-well plates with an autosampler procedure according to the manufacturer's instructions. Each sample was analysed in triplicate at 340 nm with a spectrophotometer (TECAN infinite®). Samples presenting lactate concentration above the quantification linearity were diluted in deionised water. All results were normalised with a fresh culture medium used as a blank.

Online Raman spectroscopy

The acquisition of culture medium Raman spectra was performed *online* with an Rxn2 IOT Raman spectroscopy analyser (Endress Hauser) and associated Raman probe (bIO-LAB 220; Endress Hauser) kindly provided by Kaiser-Endress. The probe was placed within the DASbox® tank before set-up sterilisation. The excitation wavelength of the laser was 785 nm. A preliminary blank spectrum was acquired and lasted 15 min. The acquisition parameters were optimised to target between 50 and 80% of saturation. Thus, they were set at 40 s and 20 accumulation counts for offline calibration assays and at 50 s and 20 accumulation for online assays. After Raman spectrum acquisition, online lactate monitoring was calibrated based on offline samples. Seventy-six off-line spectra were generated from spiked fresh or spent medium samples from fibroblast's culture (See sample list in **Supplementary 2**).

Live and Dead Cells Imaging

At the end of the culture, a biopsy of the cellularised construct was cut and used for live and dead cell staining. The samples were rinsed with PBS 1X (Gibco), then immersed and incubated in 2 µM calcein green solution (Calcein, AM, cell-permeant dye, C1430, Invitrogen™) at 37°C for 30 min in the dark. The cellularised structures were then rinsed with PBS, immersed in 300 nM DAPI (4',6-Diamidino-2-Phenylindole, Dihydrochloride) (Invitrogen™, D1306) and incubated for 10 min at 37°C in the dark. Live (green calcein staining) and dead (light blue DAPI staining) cells were observed in a dark room with a fluorescence microscope (Nikon Eclipse Ts2R) equipped with 490 nm and 340 nm filters. Live cells were visible as green, fluorescent cells, and the nuclei of dead cells were stained in light blue.

Tissue dissociation and cell counting

At the end of the culture, a biopsy of the cellularised construct was cut and dissociated using a solution of collagenase A (COLLA-RO Roche) (4.5 U/mL) in PBS 1X (Gibco). The solution was warmed at 37°C in a water bath. The tissues were rinsed once with 2 mL PBS 1X (Gibco) and then weighted before being immersed in the collagenase solution (2.5 mL per cm^3 of construct). The biopsy structure was then incubated at 37°C in a water bath with vigorous agitation every 10 to 20 minutes until complete dissociation. The recovered cells were centrifuged at 300 g for 5 min, and the pellet was resuspended in 1 mL PBS. Cells were counted on a hemocytometer with 0.4% trypan blue staining for viability and live cell concentration determination.

Tissue architecture

3D architecture by Magnetic Resonance Imaging (MRI)

At the end of the culture, the bioprinted structure was fixed by incubation in AntigenFix (DiaPath, P0014) overnight at 4°C. The construct was then rinsed and kept in ethanol 70% before MRI analysis. The MRI protocol was carried out on a 7 Tesla Bruker BioSpec MR system (Bruker Biospin GbmH, Germany) equipped with a 400 mT/m maximal amplitude gradient set and controlled using a Bruker workstation interfaced with ParaVision5.1 software for data acquisition and post-processing. A transmit-receive radio-frequency body coil (outer diameter = 112 mm and inner diameter = 72 mm) was employed for *in vitro* MR image acquisition. To acquire 3D high-resolution MR images of the bioprinted, a tridimensional T2-weighted MR sequence based on the Rapid Acquisition with Relaxation Enhanced (RARE) method was obtained on transversal orientation. The acquisition parameters were as follows; Echo Time (TE): 35.8 ms, Repetition Time (TR): 600 ms, bandwidth: 75 kHz, RARE accelerator factor: 8, and average number: 2. A total of 256 slices of 273 µm slice thickness were acquired within a field of view of 3.5 x 3.5 x 3.5 cm^3, and an in-plane matrix size of 256 x 256 x 128 interpolated to 256 x 256 x 256 pixels, providing a final in-plane isotropic resolution of 137 x 137 x 137 $µm^3$. The total acquisition time was 1h1m26s.

Histological analyses

After MRI analysis, the bioprinted structure was rinsed in PBS and fixed using paraformaldehyde solution (Antigenfix DiaPath; P0014) overnight at 4°C and transferred to 70% ethanol until the next step. Paraffin embedding consisted of successive incubations at 65°C in 95% ethanol, 100% ethanol, ethanol/butanol

mix, and butanol/methylcyclohexane mixes. Each incubation lasted for 20 min. Paraffin impregnation was then performed at 56°C for 2 h. Paraffin blocks were formed using metal moulds. The dehydrated constructs were sliced into thin sections of 5 µm using a microtome. The sections were disposed of on Superfrost slides (Epredia, 12321). The sections were stained for Masson's Trichrome to observe cell repartition inside the structure. Sections were stained with Groat's hematoxylin for 1 min, Fuschin-ponceau for 3 min, G orange-phosphomolybdic acid for 3 min, and fast green for 3 min. Each staining step was followed by a water or 1% acetic acid wash. Sections were then dehydrated by rapid immersions in 70%, 95%, and 100% ethanol, and finally, slides were mounted with ExPert Mounting Medium (CellPath, SEA-1604-00A).

Tissue internal flow monitoring

Velocity Maps by Magnetic Resonance Imaging

The Magnetic Resonance Imaging (MRI) protocol was carried out on a 7 Tesla Bruker BioSpec MR system described in section 2.6.1. Synthetic microporous structures (design A or B) were 3D printed thanks to a Prusa MINI + printer (PRUSA Research, Czech Republic) using 0.1 mm resolution slicing and used as ideal objects. They were sequentially inserted in the bioreactor's chamber, leaving a gap of 2.2 mm towards the outlet wall and 2.4 mm towards 1 lateral wall. The bioreactor was then sealed and inserted inside the transmit-receive body coil positioned in the centre of the 7T MRI system (**Supplementary Fig. 2**). A flow loop was set up using a peristaltic pump, Masterflex Ismatec ISM834C. The whole set-up, including the rollers' stretch, was connected with an autoclavable translucent hose, Versilic flexible tube, Ø 3mm x Ø 6mm (228-1194-VWR). The pump speed was calibrated by mapping the display reading to the displaced weighted volume, sweeping the whole range separated by 6 sampled speeds. A linear regression model was established (coefficient of determination $R^2 = 0.993$). The hydraulic circuit was filled with stained water. The incoming flow hose was connected to one bottom orifice, while the outgoing flow hose was released in the opposite-side upper orifice. The pump was set to run the experiments with two different pump flows: 2 mL/min and 19.6 mL/min.

The velocity map sequence acquisition was carried out using the flow-imaging technique known as Flow Map, which is based on the phase contrast method [21]. Phase contrast MRI (PC-MRI) is a non-invasive imaging technique that does not require contrast agents and can provide high-resolution images of blood flow in any direction. PC MRI relies on the principle that the phase of the MRI signal is proportional to the velocity of the protons. To perform PC-MRI, two images are acquired with oppositely applied magnetic field gradients. This creates a phase difference between the two images that is proportional to the velocity of the protons. The phase difference image can then be used to calculate the velocity of the flowing fluid. The sequence was set with the following parameters: average of four images, eco time: 5 ms, repetition time: 50 ms. The maximum flow velocity measured with a given flow imaging sequence was set at 20 $cm.s^{-1}$. In comparison, the minimum flow velocity measured with the given pulse sequence parameters was set at 0.74 $cm.s^{-1}$.

Four scenarios, two velocities for two macroporous structures, were acquired sweeping consecutive sagittal planes (XY) separated by 1mm and encoding the velocity vector components in all directions (XYZ). Each acquisition was set to cover a field of view of 5 x 5 cm, represented in 256 x 256 pixel images with a resolution of 195 µm.pixel^{-1} for each direction (XYZ). The photos were encapsulated both in DICOM and 2D sequence formats. Each experiment was completed in 58 min. Morphological images were also acquired in the same sweeping positions applying the T2-weighted spin-echo sequence, with and without running flow. The post-processing protocol implemented is described in **Supplementary Data _ Velocity maps by Magnetic Resonance Imaging***).*

2.7.2 Computational fluid dynamics (CFD)

Fluid dynamics simulations were performed using the commercial finite volume-solver ANSYS Fluent2019. Based on the previous work of Pourchet et al. [22], a single-phase with laminar flow was supposed, and a steady-state approach was applied for the solving of both continuity and momentum Navier-Stokes equations (Eqs. (1) and (2)), with ρ the fluid density, **v** the fluid velocity, p the pressure, $\boldsymbol{\tau}$ the Reynolds stress tensor and **g** the acceleration due to gravity. Fluid properties were like those of water at 37°C, namely ρ = 993 kg m^{-3} and dynamic viscosity μ = 6.92 × 10^{-4} Pa.s.

$$\nabla \bullet \mathbf{v} = 0$$

1

$$\nabla \bullet (\rho \mathbf{v}\mathbf{v}) = -\nabla p + \nabla \bullet \backslash \mathrm{varvec}\bar{\bar{\tau}} + \rho \mathbf{g}$$

2

Parameters discretisation was achieved by a mesh divided into approximately 19 million tetrahedral meshes. The perfusion was performed by setting a fixed flow rate and pressure outlet corresponding to the flow inlet/outlet. All other boundaries were set as no-slip walls. Finally, solving equations used the SIMPLE method for the pressure-velocity coupling and 2^{nd-}order UPWIND schemes for pressure and momentum transport equations. Simulations were run until both a minimum criterion on residuals (< 10^{-3}) and stabilisation of the fluid velocity, the pressure outlet and the wall shear stress were reached. CFD post-treatment was performed using ANSYS CFD-Post software. According to the tissue internal flow monitoring, specific velocity flow fields were plotted to compare the experimental data with the modelled ones. The simulations were applied to Design A only (**Supplementary Fig. 1**).

Results & Discussion

The present study aimed to assess methodologies for controlling the physicochemical environment of cultured tissues and to explore the non-invasive monitoring of their evolution. Our approach centres on using 3D-printed perfused culture chambers for tissue cultivation. This strategy facilitates reaching the perfect fit between the chamber and the bio-printed structure and enables fine-tuning of the internal/external fluid dynamics and three-dimensional architectural features. Emphasis is placed on

elucidating the internal tissue structure, nutrient and oxygen transport pathways within 3D architectures, and the metabolic status of the tissue through non-destructive, contactless means, thereby proposing assessment methodologies for the late-stage evaluation of tissues before implantation. We explore and present a range of technologies sourced from both the bioproduction/bioprocess and in vivo analysis domains.

Regulated tissue physicochemical environment

Protocols were set to cultivate 3D bioprinted structures of 10.8 cm^3 (2 x 2 x 2.7 cm). Our strategy was applied to 3D structures cellularised with different cell types to select generic regulation protocols. Thus, dermis fibroblasts and Chinese Hamster Ovary (CHO) cells were cultivated in 3D bioprinted cultures for 5 to 15 days. The initial regulation protocols and control loops were transferred from standard protocols used for cell culture processes applied in pharma industries with such bioreactor vessels. In all cases, temperature and pH regulation were very well regulated with the standard bioprocess protocols. For example, in fibroblast culture, only a 0.25% deviation was observed regarding the set point for pH regulation.

On the contrary, the standard regulation protocols had to be optimised for dissolved oxygen to fit the 3D tissue needs. Adapting the regulation to suit the 3D cultivation models became imperative due to the significantly reduced cell growth rate observed in such conditions. Our prior research has already delineated this phenomenon for fibroblasts, which exhibit a proliferation rate half that observed in conventional 2D cultures (generation time of 3.5 days versus 1.7 days in 2D cultures)[19]. The team has demonstrated similar behaviour for other cell types, including CHO (Data not shown). Standard regulation protocols commonly applied in cell culture bioprocesses provided poor control of the tissue nutritive fluid environment (**see** Fig. 2 **– Top graphs A & B).** A substantial deviation of the oxygen level was observed (ranging from 50–100% of the set-point value). The oxygen level, initially regulated thanks only to positive regulation and injection of air and O_2 gas, was later better-controlled thanks to the addition of a negative regulation with N_2 in the gas mix. Once the O_2 regulation actuators were set up, it was necessary to apply several fine tunings of the PID parameters and the regulation cascades to appropriately regulate the dissolved oxygen concentration. Table 2 presents optimised PID (Proportional kp; Integral ki; Derivative kd) parameters achieved for both fibroblasts and CHO cells. For example, we reached a 13.4 %deviation in oxygen regulation for CHO cells with a PID of 10 times reduced proportional factor (kp) and 6 times increased integral factor (ki). Both evolutions in the regulation protocols allowed the reduction of dissolved oxygen deviation to the set point from 51.1 to 13.4 %in the case of the CHO cells and from 131 %to 11.5 %in the case of fibroblast cells (See Fig. 2 – bottom graphs).

Table 2

_ Regulation parameters (PID) optimisation (Proportional kp; Integral ki; Derivative kd). The column in white indicates the original PID parameters commonly set for cell culture processes, while values in the grey column are the optimised PID parameters for cellularised 3D bioprinted constructs. The regulation parameters that were significantly changed are indicated in bold. dO2 is the dissolved oxygen measured in % of air saturation.

	FIBROBLAST CULTURE		**CHO CULTURE**			
Culture system	Custom Cytosys bioreactor system		Ambr®250 High Throughput bioreactor system			
Parameter regulated	Oxygen		Oxygen regulation Cascade: Level 1		Oxygen Regulation Cascade: Level 2	
Output	Gas flow mix (Air/CO_2)	Gas flow mix ($Air/N_2/CO_2$)	Gas flow mix (N_2/Air)		O_2 added flow	
Effect	increases dO_2	increases / decrease dO_2	decreases dO_2		increases dO_2	
Maximal flow rate (mL/min)	0 / 5	0 / 5	0 / 20	0 / 20	0.1 / 80	0.01 / 80
Proportional term (kP)	2.5	**5**	0.1	**0.8**	3.5	**0.3**
Derivative term (kI)	0	0	100	99	250	249
Integral term (kD)	0.005	**0.001**	5	**7**	2	**12**

Interestingly, regulation performed when cultivating CHO or fibroblast cells in 3D demonstrates different regulation trends. Fibroblast cells, seeded at low cell densities (between 0.125 to 0.266 x 10^6 cells/ml), exhibit a more pronounced oscillation in the measured dissolved oxygen (Fig. 2.**b**). Conversely, this oscillation is significantly diminished for CHO cells seeded at 40–80 times higher cell densities (Fig. 2.**a**). In large-scale cell culture process fields, such oscillations in dissolved oxygen are commonly exploited to reach the global oxygen uptake of the cell culture. This is related to the number of cells and their intrinsic cellular oxygen consumption rate (OCR). In the present case, CHO cells are known to have a four times more active respiratory metabolism than the dermis fibroblasts[23]. Thus, monitoring dissolved oxygen oscillation could indirectly represent the 3D construct cellular content and respiratory metabolic state. Consequently, this marks the first qualitative real-time online description of the respiratory metabolism of tissue-like structures.

Moreover, this approach is a valuable tool for continuously monitoring the quality of the physicochemical tissue environment in real-time. The graphs of Fig. 2 depict instances of specific deviations and

alterations in the regulatory protocols (highlighted by red arrows). These deviations in our culture protocols represent the addition/sampling of media in the regulation vessels. The ability to accurately record such occurrences and their effects on the physicochemical cellular environment could later be leveraged to correlate with changes in tissue behaviour or to guide the culture protocols precisely, mirroring current practices in manufacturing biopharmaceutical biomolecules. This capability represents a crucial component for subsequent regulatory documentation in tissue production.

Internal structures characterisation using Magnetic Resonance Imaging (MRI)

Internal structures of on-development organs and tissues constantly change under cell activity, leading to extracellular matrix secretion and remodelling, vessels and cavities formations, tissue densification etc..... The geometry of a 3D bioprinted tissue is then expected to change during *in vitro* maturation and needs to be monitored. The only characterisation methods available so far are destructive (histology, electron microscopy) or require sample preparation (light-sheet and confocal microscopy); the evolution along maturation of internal morphological features and structures of the tissues are still out of reach. *In vivo*, magnetic resonance imaging (MRI) is the least intrusive and safest tool to monitor internal structures. In the present study, we performed an MRI follow-up of our 3D bioprinted conjunctive tissue seeded with Fibroblasts and cultivated over 15 days to evaluate non-destructive modalities. Figure 3 presents the MRI results obtained using a T2-weighted MR sequence on a 7 Tesla MRI system, allowing a high contrast between liquid and the matrix. As a first conclusion, it is now clear that 3D bioprinted cellularised hydrogels can be imaged with high resolution (137 x 137 x 137 μm^3 voxels) and without any contrast agent. Indeed, Fig. 3-A depicts the 10.8 cm^3 3D bioprinted conjunctive tissue right after printing, together with its immediate Magnetic Resonance imaging. The MRI was also straightforward, using sagittal, distal and coronal views to study and follow the on-development tissue's internal geometries (vessels and cavities).

A numerical analysis was performed to further the evaluation and exemplify the possibility of quantifying geometry modifications. The comparison between the initial STL file and the 3D structure segmented (3DSlicer, USA) from the MRI file is shown in Fig. 3-B. More than 1 million discrete positions were compared between the two files. As can be seen, 87.6% of the imaged tissue was less than 1mm (4% of the mean initial dimension) out of alignment with the initial STL. These deviations are believed to be mainly attributed to both bioprinting fidelity and sample deformation during handling but not to the MRI imaging step.

Then, to demonstrate longitudinal imaging, the same 10.8 cm^3 3D bioprinted conjunctive tissue was imaged after 16 days of maturation in a regulated bioreactor (Fig. 3-C). As expected, shape evolution was evidenced by porosity clogging, shape deformities, and matrix degradation. Comparing one sagittal view with its corresponding histological section enabled the correlation between destructive and non-destructive methods.

Magnetic Resonance Imaging (MRI) has been identified as a non-destructive and precise method for monitoring the internal structures of 3D bioprinted tissues during their *in vitro* maturation, overcoming the limitations of traditional destructive characterisation methods. High-resolution imaging without contrast agents is feasible, as demonstrated in the study's follow-up of 3D bio-printed conjunctive tissue, revealing significant alignment with initial geometrical designs and allowing for the observation of tissue development and maturation over time. This advancement offers a promising avenue for in-depth study and quantitative analysis of tissue engineering processes, marking a significant step forward in regenerative medicine.

Internal tissue flow simulation and characterisation

Dynamic feeding of tissue is a need when one wants to culture large tissues above cm^3 volume. In such cases, culture vessels should ensure a sufficient supply of oxygenated nutritive fluids to the cells, cellularising the tissues. Here, the real challenge is to supply feeding inside the 3D structures in a vascular or microvascular manner. In such cases, designing cultivation vessels is intricately linked to the capacity to qualify the flow distribution inside the tissues. We present here two complementary strategies that allow us to describe and qualify the nutritive flow path and speed within 3D architectures of 10.8 cm^3 in a non-destructive manner. The first is a simulation-based strategy using Computational Fluid Dynamics (CFD), allowing the screening of several flow configurations to select and optimise the tissue feeding strategy; the second is an MRI-based flow measurement in 3D, mapping the real flow path and quantifying flow speed in a non-destructive manner.

CFD simulation of the nutritive flow path in multi-entry bioreactor

We used a simulation strategy based on CFD modelling to determine the flow paths generated in a multi-entry culture vessel. In such a case, we simulated the flow path within our 3D multi-entry culture chamber, welcoming the design of a 12 x 12 pores macroporous structure thanks to ANSYS Fluent software. Several case studies were simulated, including two inlet/outlet tubing sizes, different inlet/outlet positioning and two flow rates (Fig. 4). The conditions tested were commonly applied for bioprinted tissue cultivation conditions, namely, 2 and 20 ml/min. These simulations allowed us to identify a preferential flow path in the plan aligned with the inlet/outlet (Fig. 4.**a & Supplementary Fig. 3**). Then, investigating the effect of flow speed demonstrated an approximately 4-fold increase of the maximal velocity achieved within the porous channels. Flow distribution was also more impacted by the inlet/outlet diameter than the flow rate (Fig. 4.**b**), and the inlet position did not affect the simulated velocity distribution (Fig. 4.**c**). Altogether, these simulation studies enabling an easy screening of the flow experimental parameters (inlets/outlets diameter and flow speed, channel design, positioning of the inlets/outlets), demonstrated that CFD could further support the design of nutritive flow feeding strategy in macroporous 3D structures.

3D flow velocity mapping of multi-entry bioreactor by MRI

Validating the distribution of nutritional flow paths experimentally in a non-contact, non-destructive manner is crucial to confirm and strengthen the simulated options screened by CFD. Therefore, our research focused on utilising an imaging tool capable of quantifying flow velocities *in vivo*. In this regard, we assessed MRI to measure the actual fluid distribution and velocities within our 3D architecture precisely. To validate the computational fluid dynamics (CFD) simulation, we opted to employ an ideal 3D-printed architecture that closely resembles those used in bioprinting in terms of geometry (see **Supplementary Fig. 1**). The analytical setup is depicted in **Supplementary Fig. 2**, wherein the two 3D macroporous designs (A & B) were evaluated. Similar inlet/outlet positions and inlet flow rates to ones simulated by CFD were chosen for this experimental protocol.

The two inlet flow rates, low (2 ml/min) and high (20 ml/min), were applied and qualified with the two internal 3D geometries (Fig. 5- Design A & B). Analyses were performed in non-contact and non-destructive modes. They could be directly transferred to a nutritive flow path monitoring. Velocity MRI sequences were optimised to reach 1 mm^3 isotropic spatial resolution and to measure velocities from 200 µm/s to 10 cm/s. This resolution was achieved without a contrast agent, unlike previous *in vivo* studies, which achieved measures from 0-500 µm/s with a resolution of 0.365 x 365 x 1000 mm^3 [17].

Mapping fluid velocities with 7T-MRI identified changes in the velocity intensity distribution regarding velocity magnitude and volumetric distribution (**Supplementary Fig. 4**). As for the velocity magnitude, we could detect changes in maximal magnitude from 8 to 12 x 10^{-3} $m.s^{-1}$ between the two configurations. Indeed, for the geometry presenting the most prominent pores, a broader distribution of the velocities is observed in the volume.

A comparative analysis with the CFD numerical simulations aimed at verifying that trends in terms of the flow path and maximal intensity were consistent (Fig. 5 – **Velocity maps and CFD/MRI comparisons**). Flow paths in the central plane are consistent between the simulated and MRI-measured strategies. However, discrepancies emerge mostly at low flow rates regarding velocities, intensities, and distribution in the culture volume. These disparities were attributed to different parameters. First, the sensitivity of the MRI sequence to a lower flow rate is reduced as the sequence has been optimised for a high flow rate to allow comparison between acquisitions with different flow rates. Second, the exact geometry realised by 3D printing and its positioning in the multi-flow culture chamber induces an experimental discrepancy with the previously simulated geometry by CFD. Indeed, a gap of 2.2 mm towards the outlet wall and another 2.4 mm towards 1 lateral wall are introduced between the object and the multi-flow bioreactor chamber surface. Third, gas bubbles observed (Fig. 5 **_black dots indicated with white arrows**) on the morphological and velocity maps create artefacts that disturb the flow distribution and velocity. Still, this evaluation underscores the necessity for an experimental description of the nutritive flow path to achieve precise tissue feeding strategies and oxygenation development. Consequently, these observations confirm that both approaches are complementary to establish consistent and reliable nutritive strategies of large-scale tissues. One could serve for high-throughput, in-silico screening of architectural aspects (CFD simulation). At the same time, the other is essential for characterising and monitoring flow distribution throughout the culture process (MRI velocity maps).

Online monitoring of tissue metabolism

Taking a step further in controlling nutrient distribution within tissue architecture involves enabling real-time evaluation of the composition of the nutritive solution. Similarly, understanding the tissue-secreted by-products, especially toxic metabolic by-products, provides deeper insights into tissue physiology. Among the various technologies proposed in the cell culture bioprocess field, spectroscopic analysis of the culture supernatant shows great potential for monitoring tissue metabolism. Raman spectroscopy offers a promising approach for acquiring spectra of culture supernatant circulating within the tissue, allowing for monitoring its secretion and consumption, as demonstrated in other cell-based processes [24–26]. Sensors immersed in the culture supernatant obtain descriptive spectra in a non-destructive manner. In our study, the bIO-LAB 220 probe was implemented inside the regulation vessels to monitor the metabolite content of the tissue-perfused flow (See Fig. 1). As described in a previous publication by our team, lactic acid secretion is a reliable indicator of tissue cell growth state, demonstrated in various tissues such as dermis[19], bone, and cancerous tissues. The current study evaluated Raman spectroscopy for fibroblast and HEK293 T-seeded tissue, aiming to develop a generic monitoring tool unaffected by cell origin and metabolic activities. The challenge with tissue samples lies in their low concentrations to be measured (< 1 g/L for most conditions). At the same time, standard Raman monitoring models are typically applied to highly densified CHO suspension cells producing from 3 to 12 g/L lactate [7].

The first stage involved building a calibration between reference enzymatic lactic acid analysis and Raman spectra analysis. This part is performed thanks to chemometric and Partial Least Square modelisation using the Simca®18 software (Sartorius). Eleven batches were used to build the model to quantify secreted lactic acid from bioprinted tissue. First, 76 discrete samples were taken from culture batches running for up to 15 to 32 days of culture for 7 batches. A screening step of spectra pretreatment was applied, including mathematical smoothing or normalisation to achieve satisfactory PLS model fitting (R^2), predictive power (Q^2) and quantification error (RMSEE & RMSECV). Such screening consists of generating models to identify the best pre-treatment for spectra, achieving the highest and most robust R^2, Q^2 and the lowest RMSEE and RMSECV. The best spectra pre-treatment were a combination of baseline correction and normalisation (AsLS baseline correction & SNV) and spectra derivative 1st order. A set of 4 pre-treatments were assayed for the second step of Raman model building (Fig. 6). This second step consisted of challenging our models with external samples from four supplementary batches, gathering here 21 samples.

Figure 6 demonstrates that the optimal conditions were achieved through AsLS correction, SNV normalisation, and 1st Derivative treatment. Such preprocessing enabled precise quantification of secreted lactic acid concentration within the 0–3.5 g/L range, with a precision of 0.10 g/L. Utilising this technology, we continuously monitored the lactic acid metabolism of a 3D bioprinted dermis conjunctive tissue for 12 days in real-time. This method provided access to lactic acid concentration measurements every 16 minutes. The trend presented in Fig. 6 illustrates the hourly mean value, enabling the

identification of media renewal throughout the process (indicated by black arrows) and tracking the overall trend of lactic acid secretion, which has previously been correlated with dermis fibroblast growth in prior studies [19]. This correlation allows for the prediction of tissue proliferation phases (lag-, growth, death phases) on a global scale.

These findings align with those reported in the literature for large-scale industrial cell-culture processes, where Raman spectroscopy has become a standard tool for metabolic monitoring. Our study is a significant proof-of-concept for extending online bioprocess sensors to tissue engineering and tissue culture. This concept could include other commonly quantified molecules in cell culture processes using Raman spectroscopy, such as glucose, amino acids[27,28], or secreted proteins[29,30]. However, the requirement for an extensive but minimal number of discrete samples, representing sufficient variability to construct calibration and validation models, may hinder this technology's rapid and easy deployment in the regenerative medicine (RM) field. Nevertheless, efforts to generalise models for metabolic targets across various tissue types could significantly advance our understanding of tissue metabolic activity.

Conclusion

Integrating advanced technologies, exemplified by Raman spectroscopy and magnetic resonance imaging (MRI), into tissue culture represents a significant advancement with broad implications for tissue engineering and regenerative medicine. By extending online bioprocess sensors from large-scale industrial cell-culture processes to tissue engineering, we demonstrate the potential for real-time monitoring and precise tissue physiology and metabolism characterisation. First, our study, exemplified by our comparative analysis with computational fluid dynamics (CFD) simulations and MRI velocity mapping, highlights the complementary nature of simulation-based and experimental strategies in achieving precise tissue feeding and oxygenation. Furthermore, MRI emerges as a non-destructive and accurate method for longitudinally monitoring tissue development and maturation, offering significant advantages over traditional destructive characterisation methods. Our findings also shed light on the dynamic regulation of tissue culture protocols, facilitating continuous monitoring and adjustment of the physicochemical tissue environment. Finally, corroborated by findings from large-scale industrial cell-culture processes, it underscores the utility of Raman spectroscopy as a standard tool for metabolic monitoring of tissue. These advancements mark significant strides in regenerative medicine and tissue engineering, offering promising avenues for in-depth study and quantitative analysis of tissue engineering processes, ultimately advancing the development of functional engineered tissues for various biomedical applications.

Declarations

Competing Interests

Two of the authors Kleanthis Mazarakis & Timo Schmidberger are researcher of a private company (Sartorius) which is selling the SIMCA spectra analysis software used in this study. Also, 3d.FAB team

should specify that Sartorius has financially supported part of this work with the hiring of Laura Chastagnier as a PhD student and contributed to the completion of this work by providing the SIMCA software.

Author Contribution

LC, SP, NEK, EP, SL, CL realised the experiments and generated the data. CM, YG, SL, KM, CL, EP performed data curing, analysis, models building and figures building. EP, CM, YG, CL participated in the manuscript writing. All authors reviewed the manuscript.

Acknowledgements

We express our sincere gratitude to Jean Lynce Gnanago for his pivotal role in initiating the research on MRI flow analysis during his PhD. His dedicated study forms the cornerstone of the work presented in this paper. We acknowledge Radu Bolbos and CERMEP MRI 7T for their invaluable support in facilitating the MRI acquisition for this study—special thanks to the Sartorius PAT Team for their crucial assistance in Raman's chemometric analysis. We also acknowledge Sartorius for their financial support, which contributed to completing this work, and for providing the SIMCA software. We also acknowledge Kaiser Endress-Hauser and, in particular, Thomas Perilli for the loan of Raman equipment Rxn2 and the associated probes. The collaborative efforts and support from these individuals and organisations have been instrumental in the successful execution and completion of this research project.

References

1. Gomes, M. E., Rodrigues, M. T., Domingues, R. M. A. & Reis, R. L. Tissue Engineering and Regenerative Medicine: New Trends and Directions—A Year in Review. Tissue Eng Part B Rev 23, 211–224 (2017).
2. Ramos, T. & Moroni, L. Tissue Engineering and Regenerative Medicine 2019: The Role of Biofabrication-A Year in Review. *Tissue Eng Part C Methods* 26, 91–106 (2020).
3. Kohli, N. *et al.* Bioreactor analyses of tissue ingrowth, ongrowth and remodelling around implants: An alternative to live animal testing. Front Bioeng Biotechnol 11, (2023).
4. Eshmuminov, D. *et al.* An integrated perfusion machine preserves injured human livers for 1 week. Nat Biotechnol 38, 189–198 (2020).
5. Visone, R., Talò, G., Lopa, S., Rasponi, M. & Moretti, M. Enhancing all-in-one bioreactors by combining interstitial perfusion, electrical stimulation, on-line monitoring and testing within a single chamber for cardiac constructs OPEN. doi:10.1038/s41598-018-35019-w.
6. Harcum, S. W. *et al.* PID controls: the forgotten bioprocess parameters. *Discover Chemical Engineering 2022 2:1* 2, 1–18 (2022).

7. Esmonde-White, K. A., Cuellar, M. & Lewis, I. R. The role of Raman spectroscopy in biopharmaceuticals from development to manufacturing. Anal Bioanal Chem 414, 969 (2022).
8. Hubli, G. B., Banerjee, S. & Rathore, A. S. Near-infrared spectroscopy based monitoring of all 20 amino acids in mammalian cell culture broth. Talanta 254, 124187 (2023).
9. Leferink, A. M., Van Blitterswijk, C. A. & Moroni, L. Methods of Monitoring Cell Fate and Tissue Growth in Three-Dimensional Scaffold-Based Strategies for in Vitro Tissue Engineering. Tissue Eng Part B Rev 22, 265–283 (2016).
10. Wang, N. *et al.* Label-free structural and functional volumetric imaging by dual-modality optical-Raman projection tomography. Sci Adv 9, (2023).
11. Schueth, A. *et al.* Efficient 3D light-sheet imaging of very large-scale optically cleared human brain and prostate tissue samples. *Communications Biology* 2023 *6:1* 6, 1–15 (2023).
12. Kiemen, A. L. *et al.* Tissue clearing and 3D reconstruction of digitized, serially sectioned slides provide novel insights into pancreatic cancer. Med 4, 75–91 (2023).
13. Sharma, K. *et al.* Kidney volume measurement methods for clinical studies on autosomal dominant polycystic kidney disease. (2017) doi:10.1371/journal.pone.0178488.
14. Heinemann, A., Wischhusen, F., Puschel, K. & Rogiers, X. Standard liver volume in the caucasian population. Liver Transplantation and Surgery 5, 366–368 (1999).
15. Wei, J. C. J. *et al.* Allometric scaling of skin thickness, elasticity, viscoelasticity to mass for micro-medical device translation: from mice, rats, rabbits, pigs to humans. *Scientific Reports 2017 7:1* 7, 1–16 (2017).
16. Chau, A. C. M., Hua, J. & Taylor, D. B. Analysing breast tissue composition with MRI using currently available short, simple sequences. Clin Radiol 71, 287–292 (2016).
17. He, F. *et al.* MRI-Based Interstitial Fluid Velocity Analysis for Drug Delivery Efficiency Evaluation in Tumor. Anal Chem (2023) doi:10.1021/acs.analchem.3c03678.
18. Nam, S. Y., Ricles, L. M., Suggs, L. J. & Emelianov, S. Y. Imaging Strategies for Tissue Engineering Applications. *https*://home.liebertpub.com/teb 21, 88–102 (2014).
19. Chastagnier, L. *et al.* Deciphering dermal fibroblast behavior in 3D bioprinted dermis constructs. Bioprinting 32, e00275 (2023).
20. Pragnere, S. *et al.* Quantification of cell contractile behavior based on non-destructive macroscopic measurement of tension forces on bioprinted hydrogel. J Mech Behav Biomed Mater 134, 105365 (2022).
21. Markl, M. *et al.* Advanced flow MRI: emerging techniques and applications. Clin Radiol 71, 779 (2016).
22. Pourchet, L. *et al.* Large 3D bioprinted tissue: Heterogeneous perfusion and vascularization. Bioprinting 13, (2019).
23. Wagner, B. A., Venkataraman, S. & Buettner, G. R. The Rate of Oxygen Utilization by Cells. doi:10.1016/j.freeradbiomed.2011.05.024.

24. Li, B., Ray, B. H., Leister, K. J. & Ryder, A. G. Performance monitoring of a mammalian cell based bioprocess using Raman spectroscopy. Anal Chim Acta 796, 84–91 (2013).
25. Whelan, J., Craven, S. & Glennon, B. In situ Raman spectroscopy for simultaneous monitoring of multiple process parameters in mammalian cell culture bioreactors. Biotechnol Prog 28, 1355–1362 (2012).
26. Bhatia, H., Mehdizadeh, H., Drapeau, D. & Yoon, S. In-line monitoring of amino acids in mammalian cell cultures using raman spectroscopy and multivariate chemometrics models. Eng Life Sci 18, 55–61 (2018).
27. Domján, J. *et al.* Real-time amino acid and glucose monitoring system for the automatic control of nutrient feeding in CHO cell culture using Raman spectroscopy. (2022) doi:10.1002/biot.202100395.
28. Kozma, B., Salgó, A. & Gergely, S. Journal of Pharmaceutical and Biomedical Analysis Comparison of multivariate data analysis techniques to improve glucose concentration prediction in mammalian cell cultivations by Raman spectroscopy. J Pharm Biomed Anal 158, 269–279 (2018).
29. Saint, L. *et al.* In-line and real-time prediction of recombinant antibody titer by in situ Raman spectroscopy. Anal Chim Acta 892, 148–152 (2015).
30. Berry, B. N. *et al.* Quick generation of Raman spectroscopy based in-process glucose control to influence biopharmaceutical protein product quality during mammalian cell culture. Biotechnol Prog 32, 224–234 (2016).

Figures

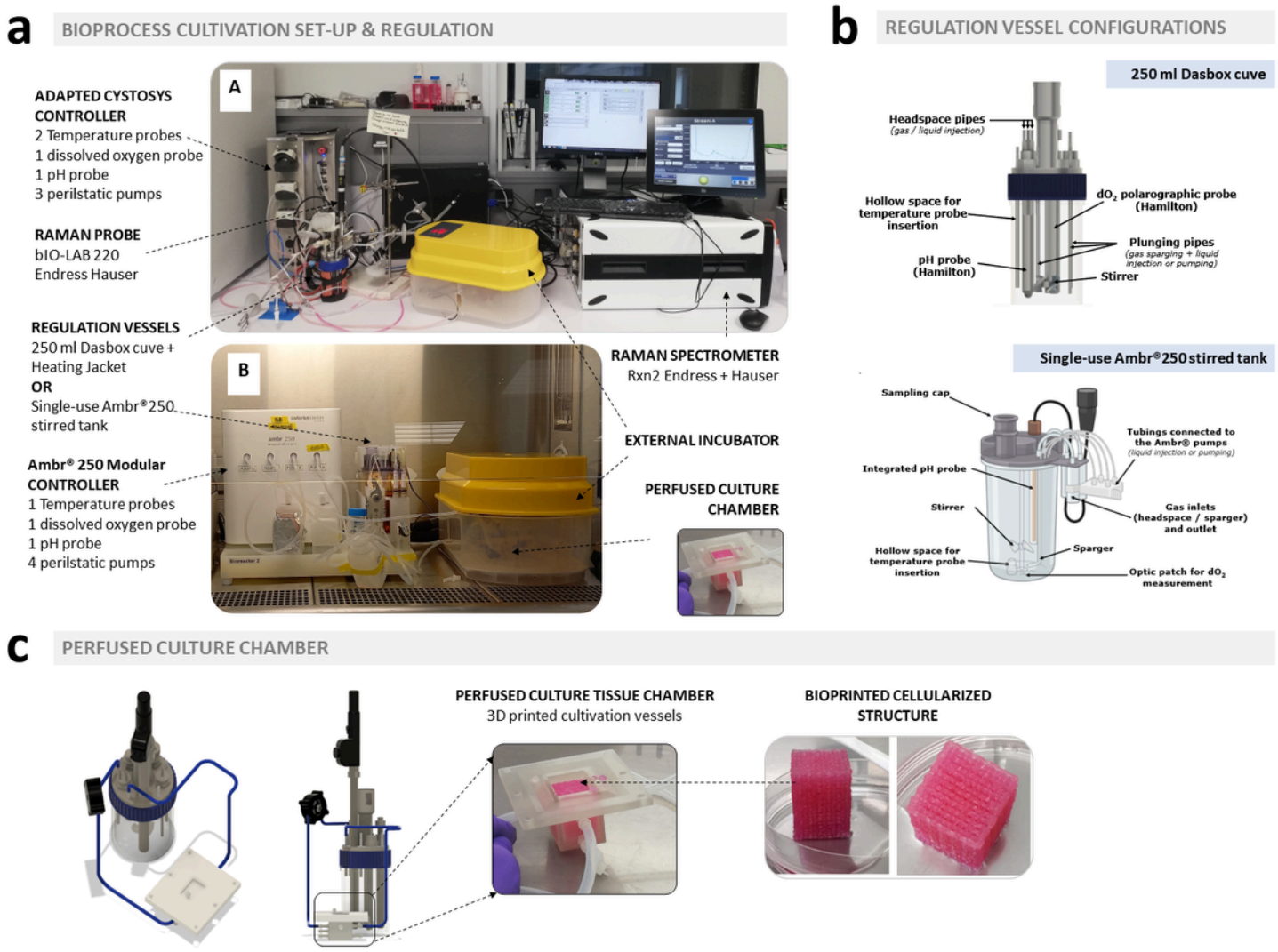

Figure 1

Tissue Bioprocess cultivation set-ups_ a. Comparative presentation of the regulation set-up proposed by the integration of stirred tanks; either the DASbox® (Eppendorf) used in the reusable stirred tank (A) or the single-use Ambr®250 stirred tank (B); with controllers (Cytosys® (Ipratech) or Ambr®250 HT control system demonstration unit (Sartorius)) and 3D printed perfused tissue culture chamber. **b.** Detailed description of the regulation vessels and their integrated sensor units. **c.** CAD design of the perfusion path and the multiflow perfused culture chamber picture.

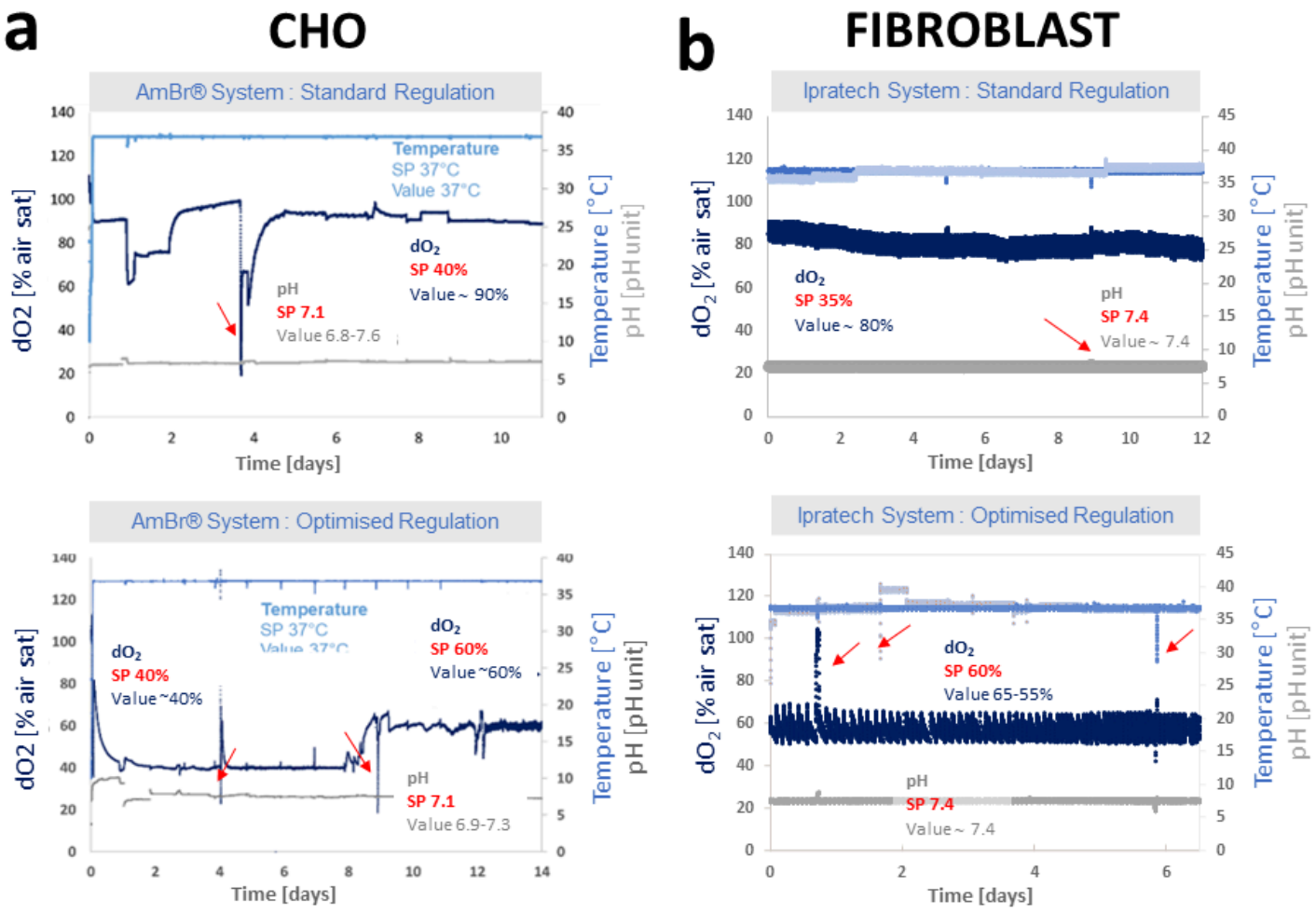

Figure 2

Online real-time regulation of tissue physicochemical environment. Monitoring culture parameters for bioprinted tissue (**a-** CHO cells conducted in a modified Ambr®250 setup / **b-** Fibroblast cells performed in a modified Ipratech setup). The top graphs present non-optimized settings and PID control based on those employed for standard pharmaceutical bioprocess cell culture. The bottom graphs present optimised settings and PID control tailored explicitly for the culture of bioprinted constructs. Red arrows identify deviations introduced due to manipulation (media addition in the regulated vessels, sampling, etc…). dO2 represents the measured dissolved oxygen.

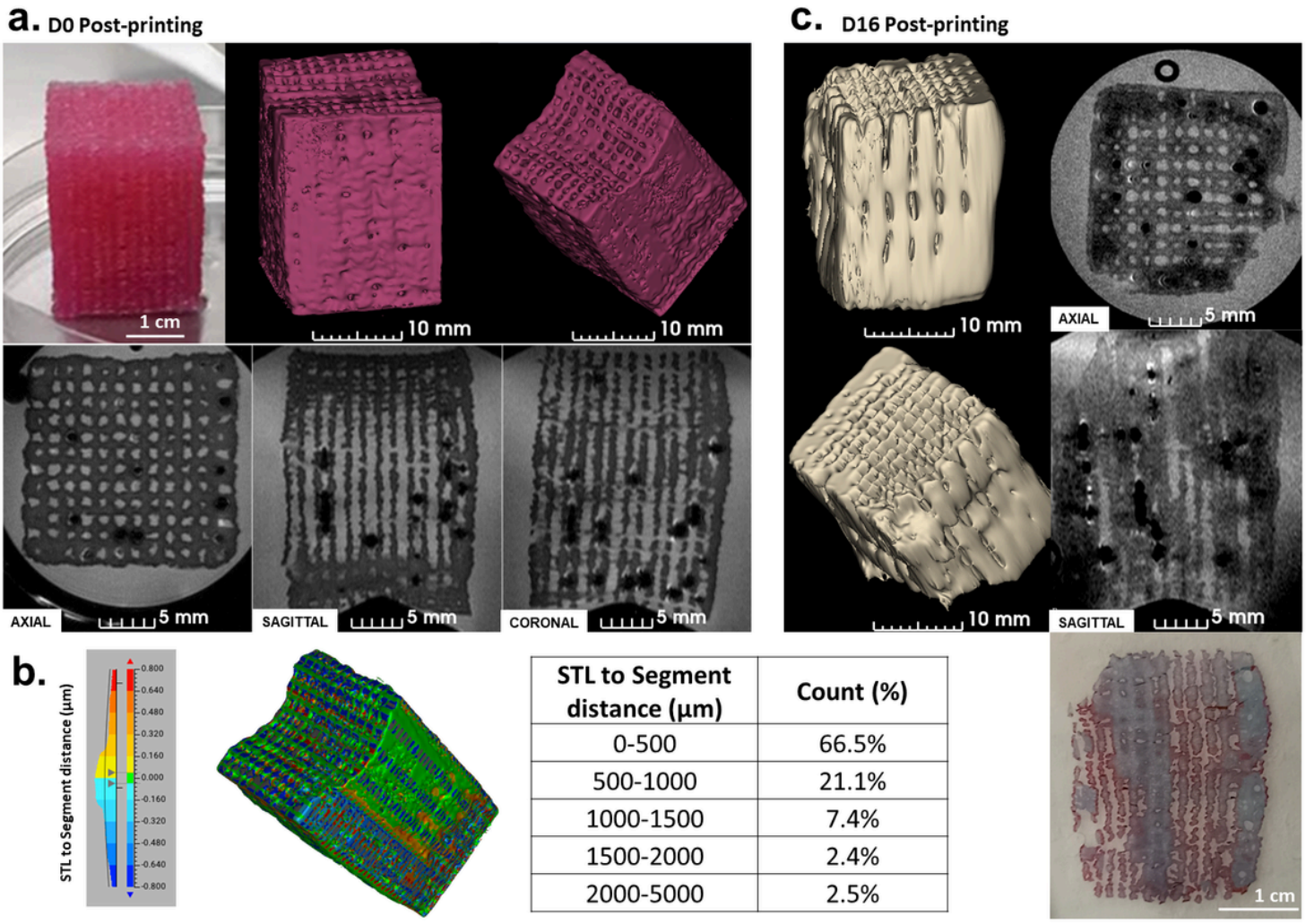

STL to Segment distance (µm)	Count (%)
0-500	66.5%
500-1000	21.1%
1000-1500	7.4%
1500-2000	2.4%
2000-5000	2.5%

Figure 3

Magnetic Resonance Imaging analysis of a 10.8 cm^3 3D bioprinted conjunctive tissue. a. Optical and MR imaging of the tissue at Day 0. **b.** Example of a numerical analysis of the tissue geometrical characterisation using volume comparisons (Artec Studio 18 (Artec 3D, Luxemburg). **c.** MRI analysis of the same tissue after 16 days of culture in a regulated bioreactor. Axial and Sagittal view and the corresponding histological section (Masson's trichrome staining).

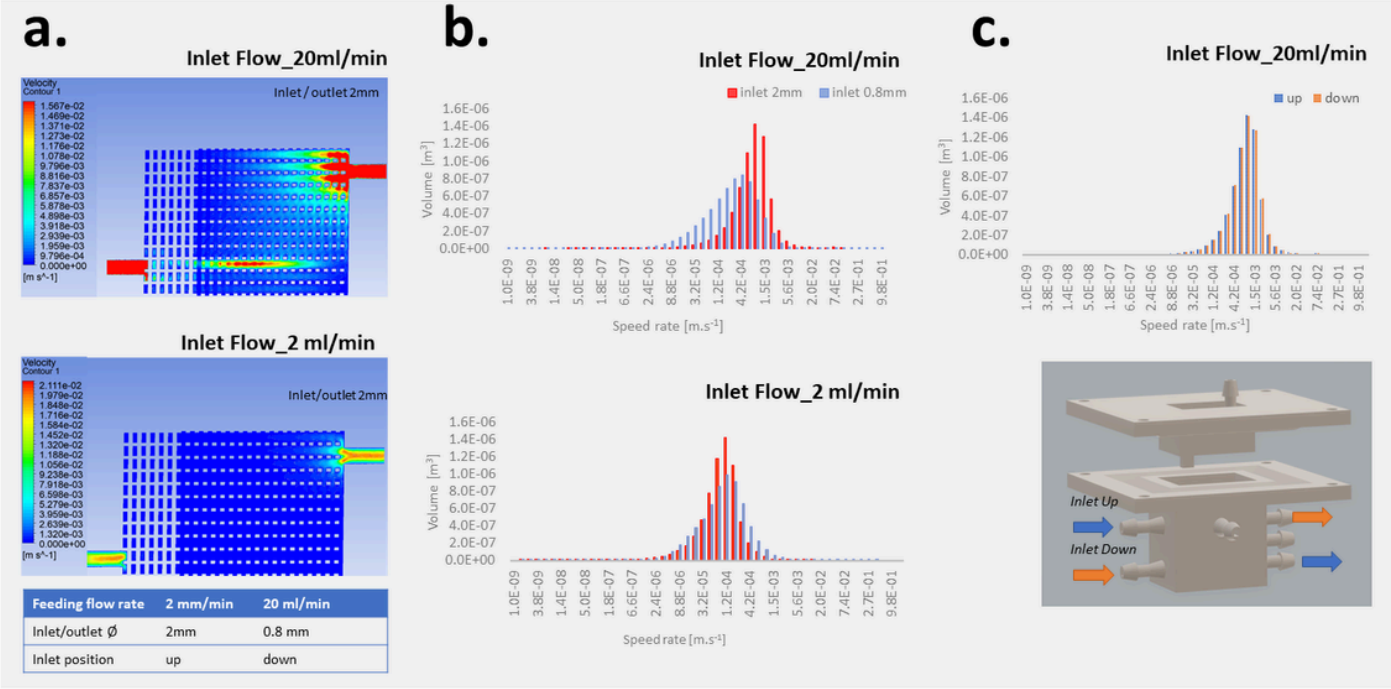

Feeding flow rate	2 mm/min	20 ml/min
Inlet/outlet Ø	2mm	0.8 mm
Inlet position	up	down

Figure 4

Numerical simulation of nutritive flow paths within 3D architectures. **a.** flow path and velocities distribution according to the inlet flow rate. **b.** The flow rate and inlet diameter impact the flow speed distribution within the 3D volume architecture. **c.** Impact of the inlet position in the 3D architecture on the flow distribution.

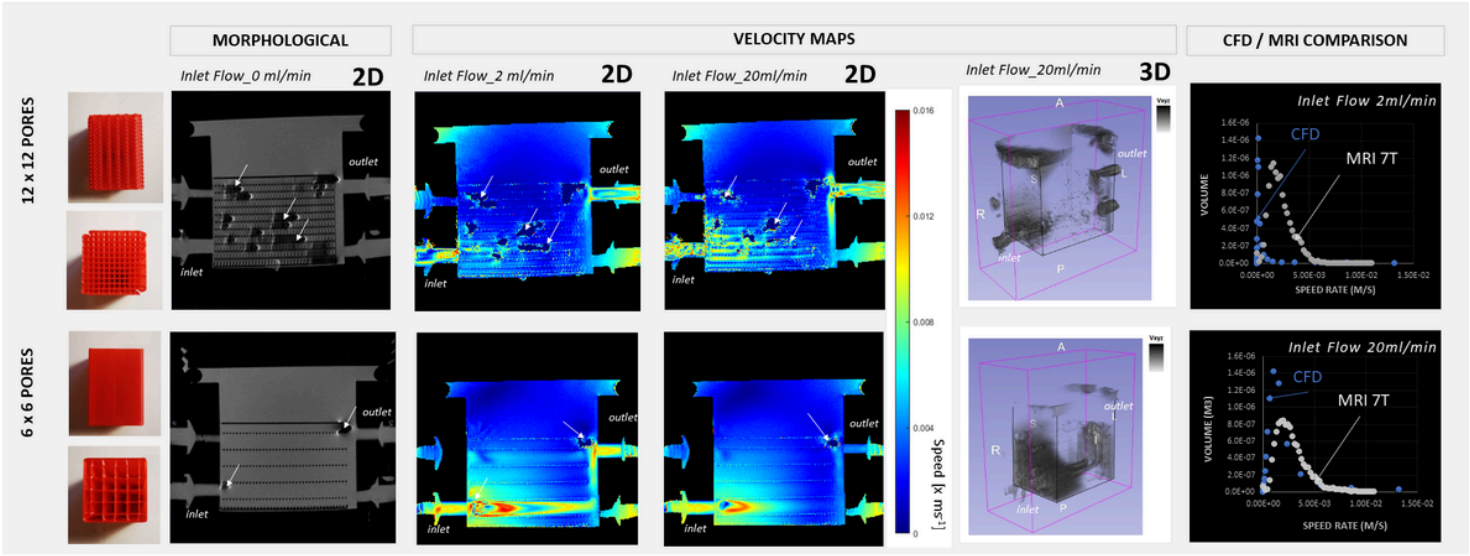

Figure 5

Non-destructive characterisation of flow distribution within the tissue by 7T MRI. Left part: 3D printed PLA models representing 3D bio-printed geometries (Design A: 12 x 12 pores / Design B: 6 x 6 pores); porosity is longitudinal**. Morphological_** Imaging of internal morphology and flow path of 3D printed

geometries acquired with T2 MRI sequence without flow. **Velocity Maps_** Planar central MRI Velocity map acquired for the two inlet flow velocities, 2 and 20 ml/min, respectively and 3D Reconstruction of 3D velocity maps for circulating inlet flow of 20 ml/min. **CFD/MRI comparison _** Velocity distribution acquired with MRI compared to CFD simulated flow rates only for Design A: 12 x 12 porous structure at the two flow rates.

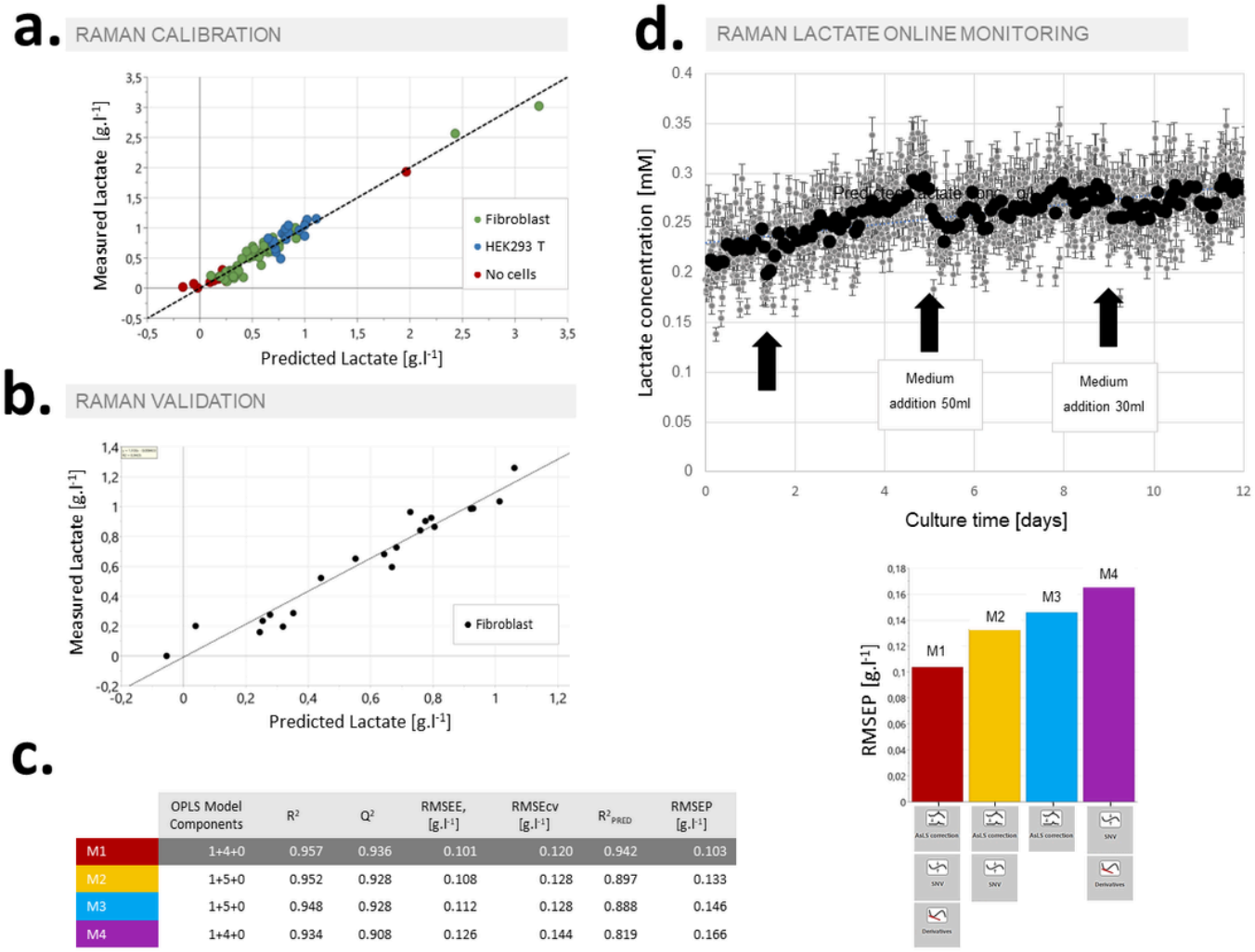

	OPLS Model Components	R^2	Q^2	RMSEE, [g.l^{-1}]	RMSEcv [g.l^{-1}]	R^2_{PRED}	RMSEP [g.l^{-1}]
M1	1+4+0	0.957	0.936	0.101	0.120	0.942	0.103
M2	1+5+0	0.952	0.928	0.108	0.128	0.897	0.133
M3	1+5+0	0.948	0.928	0.112	0.128	0.888	0.146
M4	1+4+0	0.934	0.908	0.126	0.144	0.819	0.166

Figure 6

Nondestructive and online tissue lactic acid metabolism monitoring. Correlation trends between lactic acid measured and predicted from Raman spectra for calibration (**a.)** and validation (**b.)**dataset in the case of PLS model M1. Data included used samples produced from cultures of dermis fibroblasts and kidney cells. **c.** Descriptive chemometric parameters used to classify PLS models associated with several spectrum pre-treatment combinations. **d.** Online monitoring of lactic acid was observed over time for a 12-day cultivation period from dermis fibroblasts.

Supplementary Files

This is a list of supplementary files associated with this preprint. Click to download.

- Chastagnieretal2024Supplementary.docx
- SupplementaryData.docx
- SupplementaryFigure1.tif
- Supplementaryfigure2.tif
- Supplementaryfigure3.tif
- Supplementaryfigure4.tif